

# Horizontal Visibility graphs generated by type-II intermittency

Ángel M. Núñez and Jose Patricio Gómez

*Dept. Matemática Aplicada y Estadística. ETSI Aeronáuticos, Universidad Politécnica de Madrid, Spain.*

Lucas Lacasa

*School of Mathematical Sciences, Queen Mary University of London, Mile End Road, London E1 4NS, UK*

(Dated: January 15, 2021)

In this contribution we study the onset of chaos via type-II intermittency within the framework of Horizontal Visibility graph theory. We construct graphs associated to time series generated by an iterated map close to a Neimark-Sacker bifurcation and study, both numerically and analytically, their main topological properties. We find well defined equivalences between the main statistical properties of intermittent series (scaling of laminar trends and Lyapunov exponent) and those of the resulting graphs, and accordingly construct a graph theoretical description of type-II intermittency. We finally recast this theory into a graph-theoretical renormalization group framework, and show that the fixed point structure of RG flow diagram separates regular, critical and chaotic dynamics.

PACS numbers: 05.45.Ac,05.45.Tp,89.75.Hc

## I. INTRODUCTION

Some relatively recent strategies in nonlinear analysis techniques are based on the mapping of time series into graphs according to different algorithms and criteria (see for instance [1–6]) and on the subsequent study of the associated graphs. Topological features of the associated graphs are then related to dynamical aspects of the systems that generated the series and these methods are used for feature classification based analysis of complex signals. Amongst them, the so called Horizontal Visibility Algorithm (HVA) [1, 7] can be distinguished from others by being capable of distilling time series, condensing classes of them into a single graph whose structural properties represent the basic common dynamical properties of the series. The method uncovers structural features and forms sets of time series with the same feature by their representative HV graph ensemble, excluding from the ensemble those that lack that feature. The kernel dynamics in each case is well captured by the associated graphs, such that when the HV method is applied to a time series of unknown source, inspection of the resulting graph provides basic information about its underlying dynamics. Some relevant applications of this approach include the discrimination of reversible from irreversible dynamics [8], the characterization of chaotic and stochastic signals [7, 9] or, in general, applications to series classification problems where the HV is used as the feature extraction method (see [10] for a recent review). However, from a theoretic point of view, the method is still in its infancy and graph-theoretical descriptions of nontrivial dynamics are in general open problems. This is specially important within this methodology, which has been proved to be simple enough to be addressed analytically instead of being yet another (black box) classification method, while at the same time being accurate and powerful for series classification.

In the context of low-dimensional chaos, two of the canonical routes to chaos (Feigenbaum scenario and quasiperiodic route) have been studied from this perspective and complete sets of graphs that encode the dynamics of their corresponding classes of iterated maps have been introduced and characterized [11, 12]. The third canonical route to chaos is the so called Pomeau-Manneville or intermittency route [13]. Under the generic term intermittency several dynamical behaviours with a common feature can be considered. The common feature is the alternation of (pseudoperiodic) laminar episodes with sporadic break-ups or bursts between them called intermissions. Intermittent behaviour can indeed be observed experimentally in many situations such as Belousov-Zhabotinski chemical reactions, Rayleigh-Benard instabilities, or turbulence [13–16] and has been deeply studied in the context of nonlinear sciences. As a result of this, a characterization of the onset mechanisms and main statistical properties of intermittency have been described and typified: from the classification of types I, II and III intermittency by Pomeau and Manneville [17] to other more recent types such as on-off intermittency [18] or ring intermittency [19].

The theoretical description of type-I intermittency from a Horizontal Visibility perspective has been advanced recently [20]. In the present contribution we extend the HV description to type-II intermittency and present the structural, scaling and entropic properties of the graphs obtained when the HV formalism is applied to the type-II intermittency case, further advancing the HV theory. We recall here that type-II as described by Pomeau and Manneville in their seminar paper [17] is not only of theoretical interest, but indeed constitutes a physical mechanism which has been experimentally identified, for example, in coupled nonlinear oscillators [21] or hydrodynamic systems [22].

In the following we first recall in section II the key aspects of type-II intermittency. In section III we outline the basic methodology defined as the Horizontal Visibility algorithm and apply it to the study of trajectories generated by iterated maps close to a Neimark-Sacker bifurcation, where type-II intermittency takes place. An heuristic derivation of an analytical expression for the degree distribution  $P(k; \epsilon)$  of this kind of graphs is performed. This graph measure encodes the key scaling property of type-II intermittency: the mean length  $\langle \ell \rangle$  of the laminar episodes with  $\epsilon$  manifests in network realm as a comparable scaling with the same variable of the second moment  $\langle k^2 \rangle$  of the degree distribution  $P(k, \epsilon)$ . In turn, the scaling of Lyapunov exponent  $\lambda(\epsilon)$  is recovered in network space, via Pesin-like identity, from Shannon block entropies  $h_n$  over  $P(k_1, k_2, \dots, k_n; \epsilon)$ , whose block-1 entropy  $h_1$  is only a first order approximation. In section IV we recast the family of HV graphs generated by intermittent series into a graph-theoretical Renormalization Group (RG) framework and determine the RG flows close to and at the bifurcation point. As in other transition-to-chaos scenarios [11, 12, 20], we find two trivial fixed points of the RG flow (akin to the high and low temperature fixed points in thermal phase transitions) which are the attractors of regular and chaotic dynamics respectively, together with a nontrivial fixed point associated to critical (null Lyapunov exponent) dynamics.

## II. TYPE-II INTERMITTENCY: DEFINITION AND BASIC STATISTICAL PROPERTIES

For definiteness we chose the case of type-II intermittency [13] as it develops for nonlinear iterated maps in the vicinity of a Neimark-Sacker bifurcation. As a canonical example of a discrete system exhibiting this type of dynamics let us consider the iterated complex map:

$$z_{t+1} = \alpha z_t + \mu |z_t|^2 z_t \quad (1)$$

with  $\alpha = (1 + \epsilon)e^{\varphi i}$  and  $\mu \in \mathbb{R}$ . If we rewrite the variable  $z$  in its polar form  $z = xe^{i\theta}$ , we can decompose the dynamics of the system in a rotation of its argument  $\theta$  and a nonlinear dynamics in its modulus  $x$ . We focus on the dynamics of the modulus  $x$ , which is where intermittency appears:

$$x_{t+1} = (1 + \epsilon)x_t + x_t^3 = F(x_t) \quad (2)$$

with a choice of  $\mu = 1$  for simplicity.

This one dimensional iterated map has an unstable fixed point in  $x = 0$  for  $1 \gg \epsilon > 0$ . If no additional constraints were imposed the map would diverge for initial conditions larger than zero, however, we can bound the phase space by introducing a modular congruence in the definition of this map

$$x_{t+1} = (1 + \epsilon)x_t + x_t^3 \pmod{1}. \quad (3)$$

The trajectories of this map are monotonically increasing functions up to a certain value  $0 < x_r < 1$  that fulfills  $1 = (1 + \epsilon)x_r + x_r^3$ . Then, the modular congruency reinjects it *somewhere* in the vicinity of the unstable fixed point  $x^* = 0$ , where they remain for a *certain* time (a certain number of iterations)  $t$  until they escape, go beyond  $x_r$  and are reinjected once again (see figure 1 for a graphical illustration). Reinjections close to the unstable fixed point take long journeys to depart from its neighborhood, and are experimentally seen as pseudoperiodic (laminar) phases. Chaotic bursts are actually concatenation of short trends generated out from reinjections far from the unstable fixed point (see in figure 1 the alternation between long laminar phases and chaotic bursts, governed by the location of the reinjection value).

Note that there is also a second value  $x_r < x_{2r} < 1$  very close to 1 that fulfills  $2 = (1 + \epsilon)x_{2r} + x_{2r}^3$  from which the trajectories are also reinjected in the vicinity of  $x = 0^+$ . As a numeric guide, for  $\epsilon = 10^{-3}$   $x_r = 0.68204\dots$  and  $x_{2r} = 0.99975\dots$ . This map densely fill the phase space  $[0,1]$  and evidence sensitivity to initial conditions for  $\epsilon > 0$ , regular dynamics for  $\epsilon < 0$  [13] and criticality at  $\epsilon = 0$ .  $\epsilon$  actually determines the distance of the system to the bifurcation.

A paradigmatic feature of type-II intermittency is the scaling of the mean length of the laminar trends  $\langle \ell \rangle \sim \epsilon^{-1}$ . This scaling is suggested by assuming the laminar trends to start at a  $x_0 \lll 1$  close enough to the fixed point of our map ( $x^* = 0$ ), such that

$$x_1 = (1 + \epsilon)x_0 + x_0^3 \approx (1 + \epsilon)x_0, \quad x_0 \lll 1. \quad (4)$$

This lead us by recurrence to

$$x_\ell \approx (1 + \epsilon)^\ell x_0 = [1 + \ell\epsilon + \mathcal{O}(\epsilon^2)]x_0 \approx (1 + \ell\epsilon)x_0 \quad (5)$$

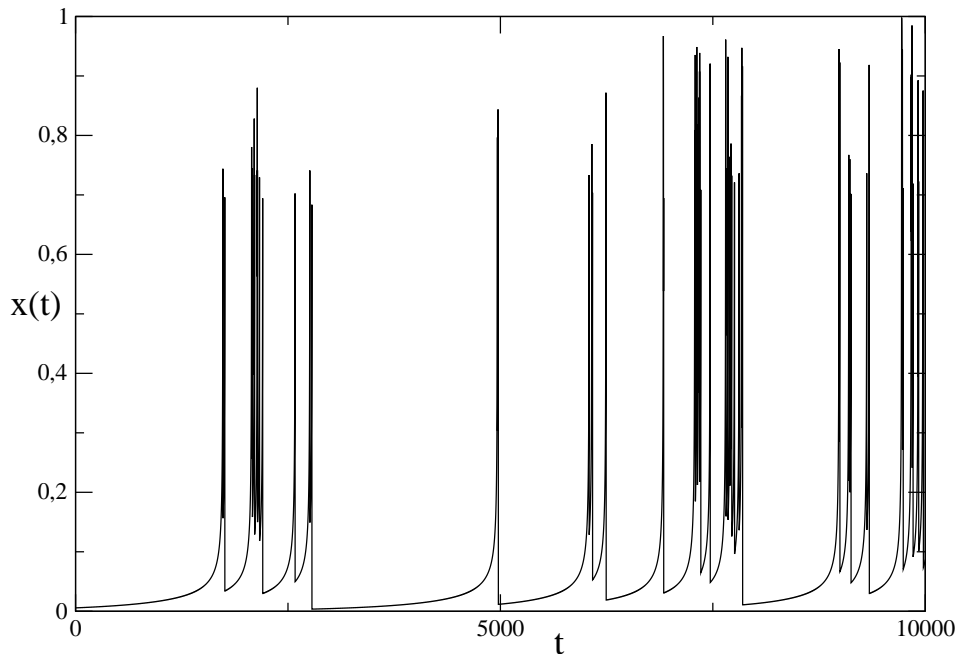


FIG. 1: A sample trajectory of the map defined in equation 3, with  $\epsilon = 10^{-3}$ . In type-II intermittency, trajectories monotonously increase until reinjection takes place. Reinjections close to the unstable fixed point take long journeys to depart from its neighborhood, and are experimentally seen as pseudoperiodic (laminar) phases. Chaotic bursts are actually concatenation of short laminar trends generated out from reinjections far from the unstable fixed point.

with  $x_\ell$  the value at which we can consider the laminar trend is over. From the former expression we get:

$$\ell \approx \frac{1}{\epsilon} \left( \frac{x_\ell}{x_0} - 1 \right) \quad (6)$$

and averaging  $\ell$  for different initial values  $x_{0_i}$  of the trend, we get

$$\langle \ell \rangle \approx \lim_{n \rightarrow \infty} \frac{1}{n} \sum_{i=1}^n \frac{1}{\epsilon} \left( \frac{x_\ell}{x_{0_i}} - 1 \right) = (\langle x_0^{-1} \rangle x_\ell - 1) \epsilon^{-1}, \quad \langle x_0^{-1} \rangle = \lim_{n \rightarrow \infty} \frac{1}{n} \sum_{i=1}^n \frac{1}{x_{0_i}}. \quad (7)$$

However, note that the definition of a laminar trend is somewhat ad-hoc, as we shall define what we consider to be such a phase, that is, when do we consider that the trajectory has escaped laminarity. Accordingly, the mean length of laminar trends  $\langle \ell \rangle$  is not a variable that directly contains information particularly relevant from the point of view of the graph theoretical description as we shall later see. A more objective measure is the time  $t$  between reinjections (or its mean value  $\langle t \rangle$ ). An expression for this variable  $t$  as a function of the initial value  $x_0$  can be found by taking the continuous limit and traducing our map to a flow:

$$x_{t+1} - x_t \approx \frac{dx}{dt} = x(\epsilon + x^2) \Rightarrow \int_{x_0}^{x_r} \frac{dx}{x(\epsilon + x^2)} = \int_{t_0}^t dt. \quad (8)$$

Assuming a relatively small initial time ( $t - t_0 \approx t$ ) this integration is straightforward and lead us to the following expression:

$$t(x_0, \epsilon) = \frac{1}{\epsilon} \log \frac{x_r \sqrt{\epsilon + x_0^2}}{x_0 \sqrt{\epsilon + x_r^2}} \quad (9)$$

where  $x_0$  is the initial or so called reinjection value (see fig. 2). If, on this expression, we make the substitution  $x_r = x_\ell \ll 1$  we can recover by approximation the expression found in eq. 6. A probability density function  $g(t)$

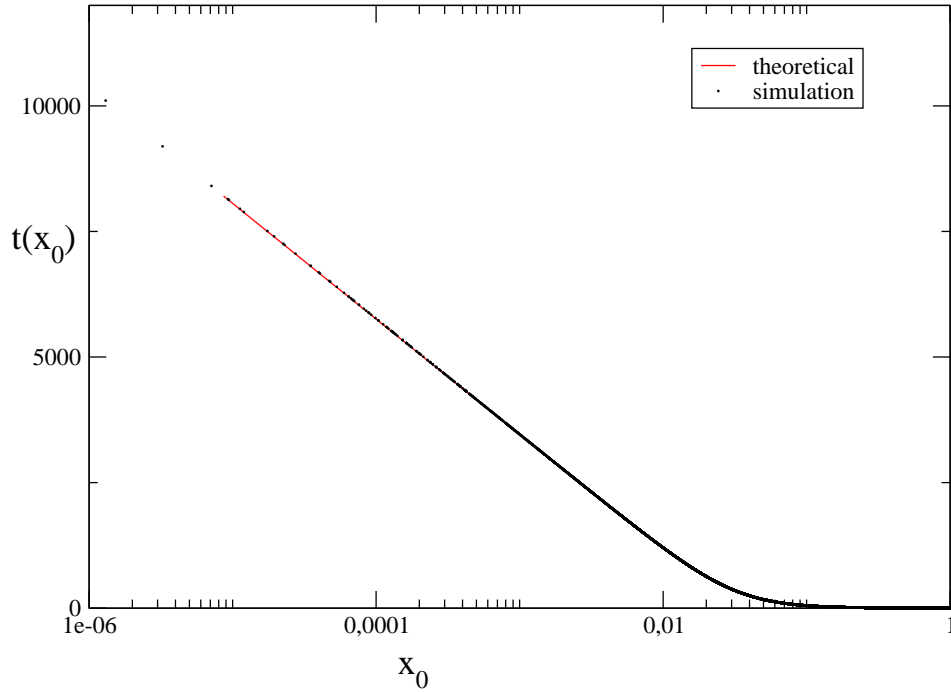


FIG. 2: Reinjection time  $t(x_0)$  for the map defined in equation 3, with  $\epsilon = 10^{-3}$  (see fig. 1). Red curve stands for the theoretical expression deduced in eq. 9. Black circles are direct numerical measures in a trajectory of length  $T = 10^7$ .

can now be deduced for the reinjection time  $t$  from the corresponding pdf  $f(x_0)$  of the reinjection values  $x_0$ , since we know that:

$$g(t)dt = f(x_0)dx_0 \Rightarrow g(t) = f[x_0(t)] \left| \frac{dx_0(t)}{dt} \right|. \quad (10)$$

From eq. 9 we have that

$$x_0(t, \epsilon) = \frac{\epsilon^{1/2}}{\sqrt{ae^{2\epsilon t} - 1}}, \quad a = \frac{\epsilon + x_r^2}{x_r^2}. \quad (11)$$

In absence of a more detailed description, we may assume in a first approximation that  $f(x_0)$  is reasonably uniformly distributed in the interval  $[0,1]$  which takes the role of the phase space of our system ( $x_0 \rightarrow U[0,1] \Rightarrow f(x_0) = 1$ ). This yields the following density:

$$g(t) = f[x_0(t)] \left| \frac{dx_0(t)}{dt} \right| = a\epsilon^{3/2} \frac{e^{2\epsilon t}}{(ae^{2\epsilon t} - 1)^{3/2}} \approx \begin{cases} \frac{a\sqrt{\epsilon}}{2} t^{-1}, & t_m \gg t \\ \frac{\epsilon^{3/2}}{\sqrt{a}} e^{-\epsilon t}, & t_m \ll t, \end{cases} \quad (12)$$

where  $t_m$  is a characteristic time scale for which we can consider that the function behaves as a power law for short times  $t$  ( $t_m \gg t$ ) and exponentially for long times  $t$  ( $t_m \ll t$ ). If we calculate the mean value  $\langle t \rangle$  with this approach for short and long times, we obtain:

$$\begin{aligned} \langle t \rangle &= \int_{t_0}^{\infty} tg(t)dt \approx \frac{a\sqrt{\epsilon}}{2} \int_{t_0}^{t_m} dt + \int_{t_m}^{\infty} \frac{\epsilon^{3/2}}{\sqrt{a}} te^{-\epsilon t} dt = \\ &= \frac{at_m}{2} \epsilon^{1/2} + \frac{t_m e^{-\epsilon t_m}}{\sqrt{a}} \epsilon^{1/2} + \frac{e^{-\epsilon t_m} - 1}{\sqrt{a}} \epsilon^{-1/2} \sim \epsilon^{-1/2}, \end{aligned} \quad (13)$$

which exhibits a scaling with  $\epsilon$  that however quantitatively differs from the one found for  $\ell$  (again,  $t_m - t_0 \approx t_m$ ). We can recover the scaling for  $\ell$  with this approach just by assuming that, in order a trend to be considered as laminar,

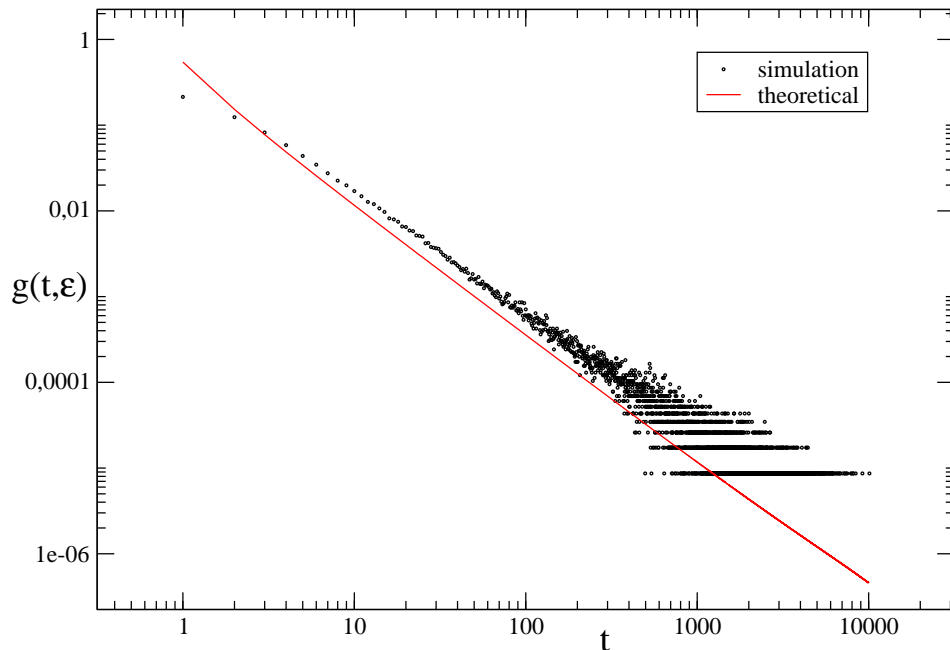


FIG. 3: Log-log plot of the probability density function of times to reinjection  $g(t; \epsilon = 10^{-3})$  for the map defined in equation 3. Red curve stands for the theoretical approximation. Black dots are extracted from the simulation of a trajectory of length  $L = 10^7$ .

the reinjected value has to be in the vicinity of the fixed point:  $x_0 \in (0, b]$ ,  $b \sim \sqrt{\epsilon}$  or otherwise,  $f(x_0)$  must be a reasonably uniform pdf:  $x_0 \rightarrow U[0, \sqrt{\epsilon}] \Rightarrow f(x_0) = 1/\sqrt{\epsilon}$ . The pdf,  $g(\ell)$ , that we obtain in this case is slightly different:

$$g(\ell) = f[x_0(\ell)] \left| \frac{dx_0(\ell)}{d\ell} \right| = 2\epsilon \frac{e^{2\epsilon\ell}}{(2e^{2\epsilon\ell} - 1)^{3/2}} \approx \begin{cases} \ell^{-3/2}, & \ell_m \gg \ell \\ \frac{\epsilon}{\sqrt{2}} e^{-\epsilon\ell}, & \ell_m \ll \ell \end{cases} \quad (14)$$

This new pdf predicts a scaling for the mean length of the laminar trend of the form:

$$\begin{aligned} \langle \ell \rangle &= \int_{\ell_0}^{\infty} \ell g(\ell) d\ell \approx \int_{\ell_0}^{\ell_m} \ell^{-1/2} d\ell + \int_{\ell_m}^{\infty} \frac{\epsilon}{\sqrt{2}} \ell e^{-\epsilon\ell} d\ell = \\ &= 2\sqrt{\ell_m} + \frac{\ell_m e^{-\epsilon\ell_m}}{\sqrt{2}} \epsilon + \frac{e^{-\epsilon\ell_m} - 1}{\sqrt{2}} \epsilon^{-1} \sim \epsilon^{-1}. \end{aligned} \quad (15)$$

where  $\ell_m - \ell_0 \approx \ell_m$ . A comparison of these expressions with the results of numerical simulations is shown in figure 3. Note that, if we expand our interval of initial conditions in the reinjection to the whole phase space  $[0, 1]$ , we recover  $t$  ( $\lim_{b \rightarrow 1} \ell = t$ ).

### III. TRANSFORMATION OF INTERMITTENT TIME SERIES INTO HORIZONTAL VISIBILITY GRAPHS

The Horizontal Visibility (HV) algorithm [7] assigns each datum  $x_t$  of a time series  $\{x_t\}_{t=1,2,\dots}$  to a node  $n_t$  in its associated HV graph (HVg), where  $n_t$  and  $n_{t'}$  are two connected nodes if  $x_t, x_{t'} > x_\tau$  for all  $\tau$  such that  $t < \tau < t'$ . The resulting are outerplanar graphs connected through a Hamiltonian path [24] whose structural properties capture the statistics enclosed in the associated series [10]. A relevant measure is the degree distribution  $P(k)$ , that accounts for the probability of a randomly chosen node to have degree  $k$ , which has been showed to encode key dynamical properties such as fractality, chaoticity or reversibility to cite some [10].

For illustrative purposes, in figure 4 we represent a sketch of a type-II intermittent series along with its associated HV graph. At odds with the phenomenology of type-I intermittency, whose mapping consisted of several repetitions

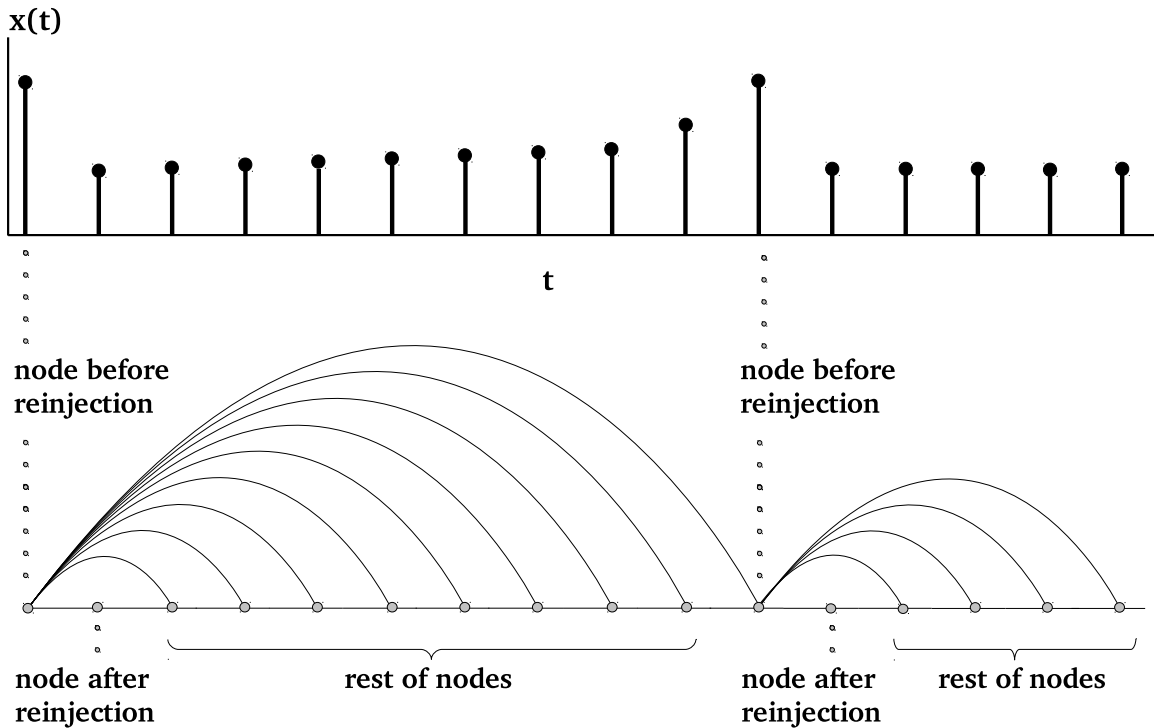


FIG. 4: Sketch of an intermittent trajectory along with its associated HV graph. Nodes 'before reinjection' correspond to values in the trajectory which have 'visibility' over the values until the next reinjection. Nodes just after reinjection correspond to values in the trajectory which are bounded by two higher values.

of a  $T$ -node motif (periodic backbone of period  $T$  associated to the ghost of the period 3 series) linked to the first node of the following laminar trend and interwoven with the chaotically connected nodes associated to the chaotic bursts between laminar trends [20], the case of type-II lacks any periodic backbone or chaotic burst, and consists of nodes associated to reinjections and nodes linked to the last node of the previous reinjection. That is, the method naturally distinguishes reinjections from each other and do not include the (nonetheless ambiguous) distinction between laminarity and burstiness.

Accordingly, we can classify nodes in three different categories (see fig. 4):

- nodes located just before a reinjection  $n_{r-}$ , whose degree distribution will be later discussed in detail,
- nodes located just after a reinjection  $n_{r+}$ , with a trivial degree distribution ( $P_{r+}(k=2) = 1$ ) and
- the rest of the nodes  $n_t$ , whose degree distribution is also trivial ( $P_t(k=3) = 1$ ).

Based on these observations, in what follows we derive some topological properties of these graphs and will show that they indeed incorporate the main statistical properties of type-II intermittency.

### A. Degree distribution $P(k)$

Consider the degree distribution  $P(k)$ , that describes the probability that a randomly chosen node of a graph has  $k$  links (degree  $k$ ). The previous features allow us to decompose the degree distribution of type-II intermittency graphs as a weighted sum of the aforementioned contributions:

$$P(k) = f_r P_{r-}(k) + f_r P_{r+}(k) + (1 - 2f_r) P_t(k), \quad (16)$$

where  $f_r$  is the reinjection fraction

$$f_r = \lim_{\tau \rightarrow \infty} \frac{n_r}{\tau}, \quad (17)$$

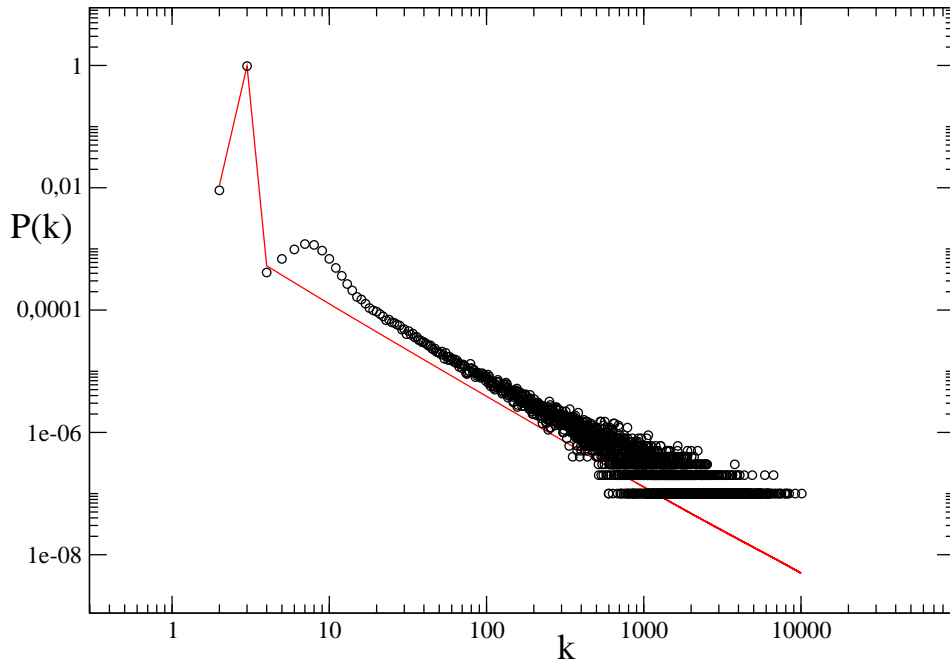


FIG. 5: (Circles) Log-log plot of the degree distribution  $P(k)$  of the Horizontal Visibility graph (HVG) mapped from a trajectory generated by equation 3 for  $\epsilon = 10^{-3}$ . (Red curve) theoretical expression for the same distribution as presented in eq. 16.

and  $n_r$  is the number of reinjections that have occurred up to time  $\tau$ .

On the other hand, the degree of the nodes before a reinjection can be decomposed in two different contributions  $k = t + k'$ . The first term  $t$  consists on the visibility the node has over the following laminar trend up to the next reinjection and it is distributed like  $P_{r-}^t(t) \approx g(t)$ . The second term  $k' = k - t$  comes from the visibility the node has over the rest of the reinjections and its distribution can be supposed to be the characteristic exponential distribution found in HVG's that come from stochastic/chaotic processes like a reinjection:  $P_{r-}^r(k) = \delta(k - k')e^{-\lambda k}$ ,  $k' \in \mathbb{Z}^+ - \{1\}$  [9]. We have one further consideration: by construction, the degree of these nodes has an additional restriction:  $k_{r-} \geq 4$ . As an approach, we can assume  $k \gg k'$  or, equivalently,  $k \approx t$ . Therefore, the degree distribution for these nodes turns out to be:

$$P_{r-}(k) \approx \int_0^k P_{r-}^t(t)P_{r-}^r(k-t)dt = g(t), \quad k = t \quad (18)$$

In figure 5 we plot in log-log the approximate theoretical expression for the degree distribution  $P(k, \epsilon)$ , for a concrete value of  $\epsilon = 10^{-3}$ , along with the numerics.

### B. Variance $\sigma_k^2 = \langle k^2 \rangle - \langle k \rangle^2$

In this section we are going to verify our previous hypothesis  $P_{r-}(k) \approx g(t)$  by deducing an expression for the mean value of the degree distribution  $\langle k \rangle$ , and we are going to analyze how the second order moment of the distribution  $\sigma_k^2$  inherits the scaling of  $\langle \ell \rangle$ . Let us start with the mean degree  $\langle k \rangle$ . Recall that HV graphs associated to generic aperiodic series tend, as size increases, to a constant mean degree  $\langle k \rangle = 4$  [23] and that HVgs are, by construction, connected graphs where node  $i$  has degree  $k \geq 2 \forall i$  (they have a Hamiltonian path). Then,

$$\langle k \rangle = \sum_{k=2}^{\infty} kP(k) = (1 - 2f_r) \cdot 3 + f_r \cdot 2 + f_r \sum_{k=4}^{\infty} kP_{r-}(k) = 4 \Rightarrow \sum_{k=4}^{\infty} kP_{r-}(k) = 4 + f_r^{-1} = \langle k_{r-} \rangle. \quad (19)$$

This expression tell us that the mean value of the connectivity of the nodes before reinjection  $\langle k_{r-} \rangle$  behaves as the inverse of the reinjection fraction  $f_r^{-1}$ . Moreover, we can express the reinjection fraction as:

$$f_r = 1 - \lim_{\tau \rightarrow \infty} \frac{n_r \cdot \langle t \rangle}{\tau} = 1 - f_r \cdot \langle t \rangle \Rightarrow f_r^{-1} = \langle t \rangle + 1 \Rightarrow \langle k_{r-} \rangle = \langle t \rangle + 5 \quad (20)$$

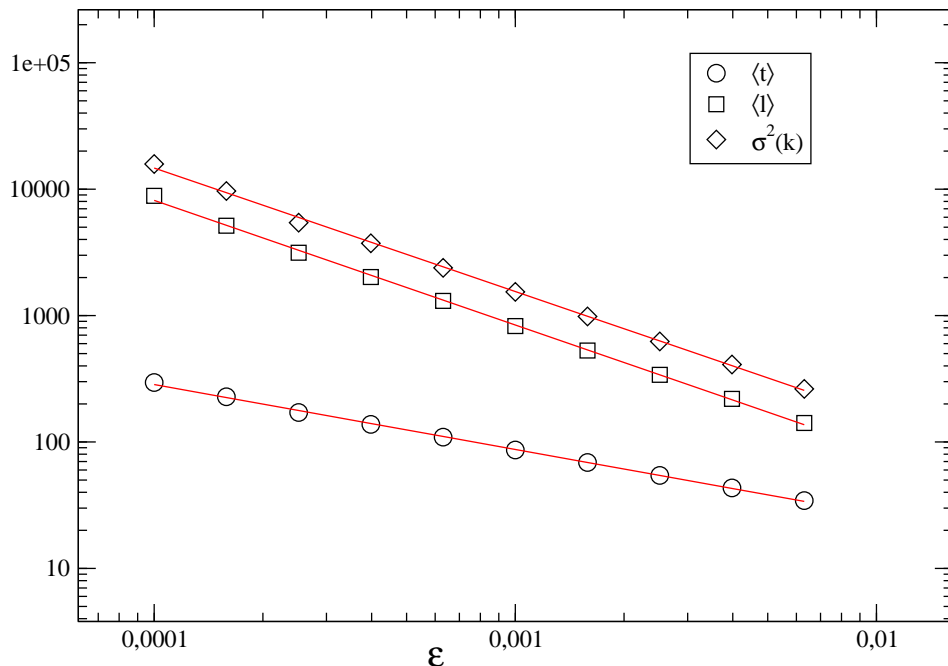


FIG. 6: Log-log plot of  $\langle t \rangle$  (circles) and  $\langle \ell \rangle$  (squares) as a function of  $\epsilon$ , numerically calculated from time series of  $10^7$  data. Diamonds correspond to the variance of the degree distribution of the associated HV graph (numerical results). In each case, solid lines are the predicted analytical scaling  $\langle t \rangle \sim \epsilon^{-1/2}$  (eq. 13),  $\langle \ell \rangle \sim \epsilon^{-1}$  (eq. 15) and  $\langle k^2 \rangle - \langle k \rangle^2 \sim \epsilon^{-1}$  (eq. 22), in good agreement with the numerics.

for which we have assumed that the number of nodes between reinjections is quite the same as the number of reinjections multiplied by the mean value of the reinjection time ( $N_t = n_r \cdot \langle t \rangle$ ), which gives a compact expression  $\langle t \rangle = \langle k_{r-} \rangle - 5 \sim \epsilon^{-1/2}$  that indicates the behaviour of  $P_{r-}(k)$  and  $g(t)$  coincides up to first order, and that  $f_r$  goes to zero as  $\epsilon^{1/2}$ .

If we now move to the second order moment, we get:

$$\sigma_k^2 = \langle k^2 \rangle - \langle k \rangle^2 = \sum_{k=2}^{\infty} k^2 P(k) - 16 = f_r \sum_{k=4}^{\infty} k^2 P_{r-}(k) + 7(1 - 2f_r), \quad (21)$$

and following our hypothesis we can approximate

$$\begin{aligned} \sum_{k=4}^{\infty} k^2 P_{r-}(k) &\approx \int_{t_0}^{\infty} t^2 g(t) dt \approx \frac{a\sqrt{\epsilon}}{2} \int_{t_0}^{t_m} t dt + \int_{t_m}^{\infty} \frac{\epsilon^{3/2}}{\sqrt{a}} t^2 e^{-\epsilon t} dt = \\ &= \frac{at_m^2}{2} \epsilon^{1/2} + \frac{2}{\sqrt{a}} \epsilon^{-3/2} \sim \epsilon^{-3/2}, \end{aligned}$$

where the last formula requires small values of  $\epsilon$  and  $t_m - t_0 \approx t_m$ . As  $f_r \sim \epsilon^{1/2}$  for small values of  $\epsilon$ , in this low limit we have a leading order of

$$\sigma_k^2 \sim \epsilon^{-1} \quad (22)$$

which reproduces the expected scaling (see figure 6 for a comparison with numerics). We conclude that the scaling of the mean length of laminar phases with  $\epsilon$  is inherited in network space by a similar scaling in the variance of the degree distribution.

### C. Scaling of Lyapunov exponent: Block entropies $h_n$

The second paradigmatic feature of type-II intermittency is the scaling of the Lyapunov exponent  $\lambda$  (which for a map  $x(t+1) = F(t)$  reads  $\lambda = \lim_{t \rightarrow \infty} \frac{1}{t} \sum_{i=0}^{t-1} \ln |F'(x_i)|$ ) with respect to the distance to criticality  $\lambda(\epsilon) \sim \epsilon^{1/2}$  [13]. Note

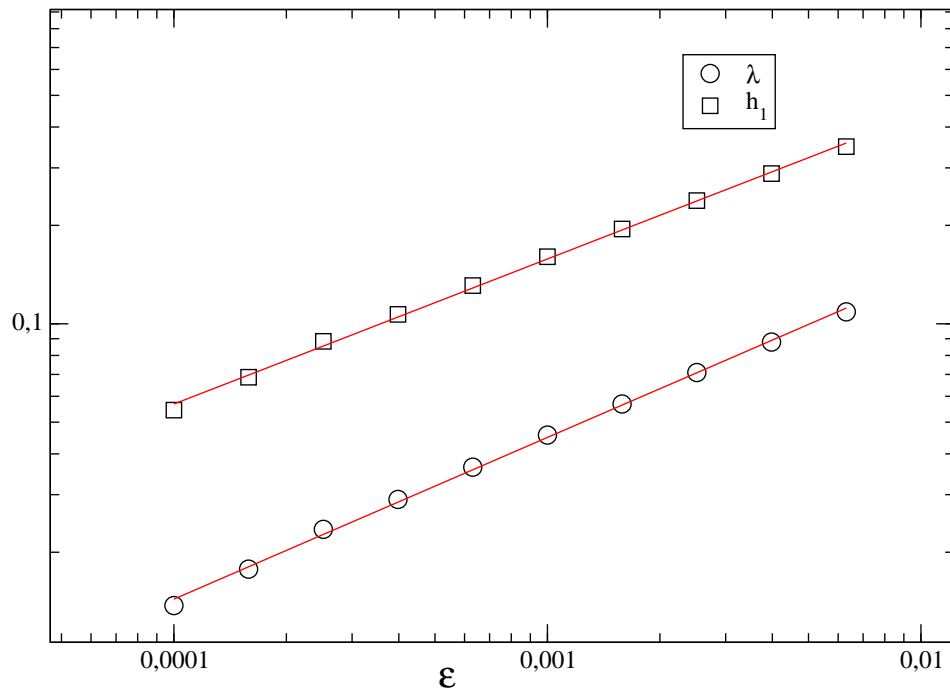


FIG. 7: (Circles) Log-log plot of the Lyapunov exponent  $\lambda$  calculated numerically from a trajectory of length  $L = 10^7$  with the expression  $\lambda = \lim_{t \rightarrow \infty} \frac{1}{t} \sum_{i=0}^{t-1} \ln |F'(x_i)|$ . Solid line is a regression with the predicted scaling:  $\lambda(\epsilon) \sim \epsilon^{1/2}$ . (Squares) Log-log plot of the block-1 graph entropy  $h_1(\epsilon)$  (see the text) of the Horizontal Visibility graph associated to the same trajectory along with a regression, whose best power law fit reads  $h_1 \sim \epsilon^{0.44}$ .

that Lyapunov exponents characterize a purely dynamical feature and, although some graph-theoretical extensions of these exponents have been recently advanced [25], it is not evident at all how to cast this dynamical behaviour into a graph-theoretical realm. However, note that Pesin identity relates positive Lyapunov exponents of chaotic trajectories with Kolmogorov-Sinai rate entropy in dynamical systems. Based on this identity, a relation between Lyapunov exponents of maps and Shannon-like entropies over the degree distribution of the associated visibility graphs has been proposed [11, 20, 23, 25]. The block-1 graph theoretical entropy  $h_1$  [20] is defined as

$$h_1 = - \sum_{k=2}^{\infty} P(k) \log P(k),$$

and block- $n$  entropies take into account of higher order statistics of blocks  $P(k_1, k_2, \dots, k_n)$ .

An approximate leading order calculation for  $h_1$  can be performed assuming  $P_{r-}(k) \approx g(t)$  and recalling that the rest of the terms in  $P(k)$  only contribute for  $k = 2, 3$ .  $h_1$  reduces to a linear combination

$$\begin{aligned} -h_1 &= f_r \log f_r + (1 - 2f_r) \log(1 - 2f_r) + \sum_{k=4}^{\infty} f_r P_{r-}(k) \log[f_r P_{r-}(k)] \\ &\approx f_r \log f_r + (1 - 2f_r) \log(1 - 2f_r) + \int_{t_0}^{\infty} f_r g(t) \log[f_r g(t)] dt \\ &= 2f_r \log f_r + (1 - 2f_r) \log(1 - 2f_r) + f_r \int_{t_0}^{\infty} g(t) \log[g(t)] dt \end{aligned} \quad (23)$$

In order to derive the leading order of  $h_1$  in  $\epsilon$ , we recall that  $f_r \sim \epsilon^{1/2}$  for small values of  $\epsilon$ . Let us pay attention to the last integral, which can be evaluated by a time scale separation for short ( $t_m \gg t$ ) and long times ( $t_m \ll t$ ) as in (12):

$$\int_{t_0}^{\infty} g(t) \log g(t) dt \approx \int_{t_0}^{t_m} \frac{a\sqrt{\epsilon}}{2} t^{-1} \log \frac{a\sqrt{\epsilon}}{2} t^{-1} dt + \int_{t_m}^{\infty} \frac{\epsilon^{3/2}}{\sqrt{a}} e^{-\epsilon t} \log \frac{\epsilon^{3/2}}{\sqrt{a}} e^{-\epsilon t} dt \quad (24)$$

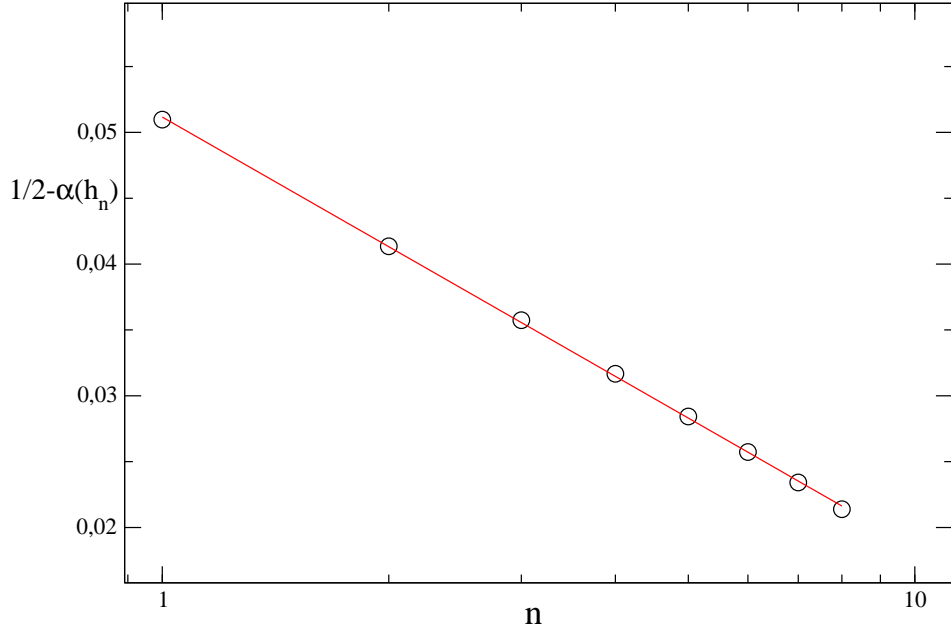


FIG. 8: (Circles) Semilog plot of the function  $(1/2 - \alpha(n))$  as a function of  $n$ , where  $1/2$  and  $\alpha(n)$  are the respective scaling exponents of the Lyapunov exponent and the block entropy  $h_n$  with respect to  $\epsilon$ . We observe that these differences decreases logarithmically with  $n$ , suggesting the presence of a graph theoretical Pesin identity (see the text).

$$\begin{aligned}
&= \frac{a\sqrt{\epsilon}}{2} \log \frac{a\sqrt{\epsilon}}{2} \int_1^{t_m} \frac{1}{t} dt - \frac{a\sqrt{\epsilon}}{2} \int_1^{t_m} \frac{\log t}{t} dt + \frac{\epsilon^{3/2}}{\sqrt{a}} \log \frac{\epsilon^{3/2}}{\sqrt{a}} \int_{t_m}^{\infty} e^{-\epsilon t} dt + \frac{\epsilon^{3/2}}{\sqrt{a}} \int_{t_m}^{\infty} t(-\epsilon e^{-\epsilon t}) dt \\
&= \frac{a\epsilon^{1/2}}{2} \log \frac{a\epsilon^{1/2}}{2} \log t_m - \frac{a\epsilon^{1/2}}{2} (\log t_m)^2 + \frac{\epsilon^{1/2}}{\sqrt{a}} \log \frac{\epsilon^{3/2}}{\sqrt{a}} e^{-\epsilon t_m} + \frac{\epsilon^{1/2}}{\sqrt{a}} e^{-\epsilon t_m} + \frac{t_m \epsilon^{3/2}}{\sqrt{a}} e^{-\epsilon t_m}. \quad (25)
\end{aligned}$$

After a brief inspection, we conclude that for small values of  $\epsilon$ , the leading term of  $h_1$  is not exactly  $\sim \epsilon^{1/2}$  but  $\sim -\epsilon^{1/2} \log \epsilon$ , what should yield an approximate scaling albeit with a smaller exponent. In figure 7 we plot in log-log the numerical results of  $h_1$  as a function of  $\epsilon$ , together with the numerics of  $\lambda(\epsilon)$  in the same range ( $\epsilon \ll 1$ ). As expected,  $h_1$  shows a reasonably similar scaling, although with a slightly smaller exponent (the numerical fit is  $\alpha \approx 0.44$ ).

If we now proceed as in [20] and we increase the size  $n$  of the block in the graph-theoretical entropy  $h_n$ :

$$h_n = -\frac{1}{n} \sum_{k_1, \dots, k_n} P(k_1, \dots, k_n) \log P(k_1, \dots, k_n). \quad (26)$$

we numerically observe a tendency in the scaling behaviour  $h_n(\epsilon) \sim \epsilon^{\alpha(n)}$  that suggests  $\lim_{n \rightarrow \infty} \alpha(n) \rightarrow 1/2$  and therefore points towards a graph theoretical Pesin identity

$$\lim_{n \rightarrow \infty} h_n = \lambda.$$

Numerical evidence for these latter results are shown in figure 8.

#### IV. GRAPH-THEORETICAL RENORMALIZATION GROUP ANALYSIS

As in previous works [11, 12, 20, 23], we can define a Renormalization Group (RG) transformation  $\mathcal{R}$  on the HV graphs  $G$  as the coarse-graining of every couple of adjacent nodes where at least one of them has degree  $k = 2$  into a block node that inherits the links of the previous two nodes. In other words, the operation removes from the graph every node of degree  $k = 2$  along with its two links. Assuming infinitely long series (in order to avoid the rescaling procedure in standard RG), in what follows we argue that the flow induced by iteratively performing this RG operation classifies dynamics coming from above and below transition, although the phase portrait turns to be very different from the one found in type-I intermittency [20].

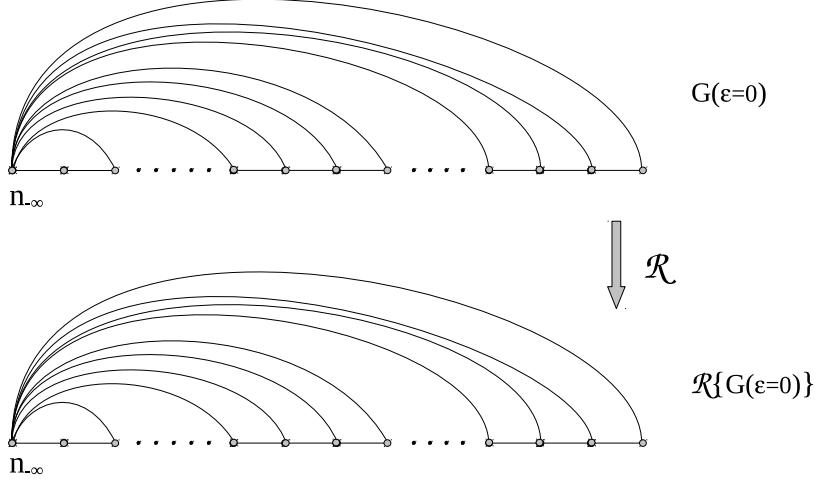


FIG. 9: Cartoon of an HV graph at criticality  $G(\epsilon = 0)$  (mapped from a trajectory at the onset of chaos in a Neimark-Sacker bifurcation,  $\epsilon = 0$  in equation 3). By construction the graph is invariant under renormalization (see the text), such that  $\mathcal{R}\{G(\epsilon = 0)\} = G(\epsilon = 0)$ . As any perturbation in  $\epsilon$  generates a RG flow that takes the HV graph away from this equilibrium towards the stable attractors (parsimoniously towards the random graph  $G_{\text{rand}}$  for positive perturbations and instantaneously to the chain graph  $G_0$  for negative perturbations),  $G(\epsilon = 0)$  constitutes an unstable fixed point of the Renormalization Group flow associated to critical dynamics on the map and acts as a boundary between regular ( $\epsilon < 0$ ) and chaotic ( $\epsilon > 0$ ) dynamics.

- When  $\epsilon < 0$ , trajectories are damped and rapidly converge to a constant series  $x(t) = 0 \forall t$ , so after a transient the associated HVG  $G_0$  will be a chain graph with  $k = 2$  for all nodes [11]. A graph which is indeed the RG attractor of regular dynamics, invariant under renormalization  $\mathcal{R}\{G_0\} = G_0$  [23] and represents a minimum for the entropy functional  $h_1 = 0$ .
- When  $\epsilon > 0$  (the situation mostly addressed in the former sections), the associated HVGs describe a flow in RG phase space where, in each iteration of the renormalization procedure, the so called 'nodes after reinjection' ( $n_{r+}$ ,  $k = 2$ ) are eliminated progressively and, step by step, the laminar phases disappear, leaving essentially a series of 'nodes before reinjection' which form mainly an uncorrelated random series. The analogous flow in graph space slowly converges towards  $G_{\text{rand}}$ , the universal HV graph associated to an uncorrelated series, which constitutes a stable fixed point of the RG flow  $\lim_{p \rightarrow \infty} \mathcal{R}^{(p)}\{G(\epsilon > 0)\} = G_{\text{rand}} = \mathcal{R}(G_{\text{rand}})$  [23]. As it has been proved that  $G_{\text{rand}}$  is a maximally entropic HV graph [23], we conclude that the RG flow  $\forall \epsilon > 0$  increases the entropy of the system as it breaks correlations.
- At the bifurcation ( $\epsilon = 0$ ) the trajectories are monotonically increasing series bounded at  $-\infty$  by a large value (the ghost of the intermittent regime), which maps into a HV graph which is itself indeed invariant under renormalization  $G_c = G(\epsilon = 0) = \mathcal{R}\{G(\epsilon = 0)\}$  (see figure 9 for a graphical illustration). Its degree distribution can be described for a graph of  $N$  nodes (where the limit  $N \rightarrow \infty$  will be taken afterwards) as  $P(k = 2) = P(k = N - 1) = 1/N$ ;  $P(k = 3) = (N - 2)/N$ , yielding also a null entropy  $h_1 = 0$  in the limit of diverging sizes. This constitutes the third fixed point of the RG flow. Note that this fixed point is different from  $G_0$ , nonetheless, they both share the same entropy. The reason is that there is no actual parsimonious trajectory connecting  $G(\epsilon = 0)$  to  $G(\epsilon < 0) = G_0$ , once you apply an infinitesimal perturbation making  $\epsilon < 0$ , after a (large transient) you reach the stationary damped solution  $x(t) = 0 \forall t$ , whose associated HVg is directly  $G_0$ . There is hence no RG flow or entropy production associated with the path. On the other hand, any positive perturbation in  $\epsilon$  is amplified in the RG flow, taking the graph to  $G_{\text{rand}}$ . We conclude that  $G(\epsilon = 0)$  is an unstable fixed point of the RG flow.

## V. CONCLUSIONS

To conclude, in this work we have further advanced the Horizontal Visibility graph theory by providing an analytical and numerical graph theoretical description of type-II intermittency route to chaos, extending previous results for type-I intermittency [20]. We have shown that the key ingredients of type-II intermittency (concrete scalings of the mean length of laminar trends and Lyapunov exponent with respect to  $\epsilon$ ) are recovered in the network realm by comparable scalings of the variance of the degree distribution and Shannon block entropy respectively. Finally, we have recasted the problem into a graph-theoretical renormalization group framework and have shown that the graph-theoretical fixed points of the RG flow distinguish regular, chaotic and critical dynamics. Whereas the trivial fixed points of the RG flow are universal attractors of regular and chaotic dynamics respectively, the unstable graph-theoretical fixed point, the RG flows and the associated entropy production paths are unique for type-II intermittency, being for instance a different scenario than what we found in type-I intermittency [20] or in other routes to chaos [12, 23].

**Acknowledgements.** We acknowledge financial support from UPM project AL13-PID-09.

- 
- [1] Lacasa L., Luque B., Ballesteros F., Luque J. & Nuño J.C., *Proc. Natl. Acad. Sci. USA* **105** (2008).
  - [2] Zhang J. & Small M., *Phys. Rev. Lett.* **96** (2006), 238701.
  - [3] Kyriakopoulos F. & Thurner S., *Lecture Notes in Computer Science* **4488** (2007).
  - [4] Xu X., Zhang J. & Small M., *Proc. Natl. Acad. Sci. USA* **105** (2008) 19601.
  - [5] Donner R. V., Zou Y., Donges J. F., Marwan N. & Kurths J., *New J. Phys.* **12** (2010) 033025.
  - [6] Campanharo A. S. L. O. , Sizer M. I., Malmgren R. D., Ramos F. M. & Amaral L. A. N., *PLoS ONE* **6** (2011).
  - [7] Luque B., Lacasa L., Luque J. & Ballesteros F., *Phys. Rev. E* **80** (2009) 046103.
  - [8] L. Lacasa, A. Núñez, É. Roldán, J. M. R. Parrondo, B. Luque, *Eur. Phys. J. B* **85**, 217 (2012).
  - [9] Lacasa L. & Toral R., *Phys. Rev. E* **82** (2010) 036120.
  - [10] A. Nuñez, L. Lacasa, J.P. Gomez and B. Luque, in *New Frontiers in Graph Theory* (ed. Y. Zhang, Intech, 2012).
  - [11] Luque B., Lacasa L., Ballesteros F. & Robledo A., *PLoS ONE* **6**, 9 (2011).
  - [12] Luque B., Núñez A., Ballesteros F. & Robledo A., *J. Nonlinear Sci.* DOI: 10.1007/s00332-012-9153-2 (2012).
  - [13] Schuster H. G. & Just, W., *Deterministic Chaos. An Introduction* (Wiley-VCH, Weinheim, 2005).
  - [14] Maurer J. & Libchaber A, *J. Physique Lett.*, **41** (1980).
  - [15] Pomeau Y., Roux J. C., Rossi A., Bachelart S. & Vidal C., *J. Physique Lett.*, **42** (1981).
  - [16] Bergé P., Dubois M., Manneville P., Pomeau Y., *J. Physique Lett.*, **41** (1980).
  - [17] Manneville P. & Pomeau Y., *Comm. Math. Phys.* **74** (1980).
  - [18] Platt N., Spiegel E. A. & Tresser C., *Phys. Rev. Lett.* **70** (1993).
  - [19] Hramov A. E., Koronovskii A. A., Kurovskaya M. K. & Boccaletti S., *Phys. Rev. Lett.* **97** (2006).
  - [20] Núñez, Á. M., Luque, B., Lacasa L., Gómez J. P. & Robledo, A., *Phys. Rev. E* **87**, 5, 052801 (2013).
  - [21] J-Y. Huang & J-J. Kim *Phys. Rev. A* **36**, 3 (1987).
  - [22] E. Ringuet, C. Rozé & G. Gouesbet *Phys. Rev. E* **47**, 2 (1993).
  - [23] Luque B., Lacasa L., Ballesteros F. & Robledo A., *Chaos* **22** (2012) 013109.
  - [24] G. Gutin, M. Mansour, S. Severini, A characterization of horizontal visibility graphs and combinatorics on words, *Physica A* **390**, 12 (2011)
  - [25] Luque B., Lacasa L., & Robledo, A.. *Phys. Lett. A* **376** (2012).
  - [26] P. Manneville, *J. Physique* **41** (1980) 1235-1243 .